Proteomics Analysis Identifies Orthologs of Human Chitinase-Like Proteins as Inducers of Tube Morphogenesis Defects in *Drosophila melanogaster*

Sandra G. Zimmerman, Gennifer E. Merrihew, Michael J. MacCoss, and Celeste A. Berg[1]
Department of Genome Sciences, University of Washington, Seattle, Washington 98195-5065
ORCID IDs: 0000-0002-2274-5471 (S.G.Z.); 0000-0003-4903-0318 (G.E.M.); 0000-0003-1853-0256 (M.J.M.)

ABSTRACT Elevated levels of human chitinase-like proteins (CLPs) are associated with numerous chronic inflammatory diseases and several cancers, often correlating with poor prognosis. Nevertheless, there is scant knowledge of their function. The CLPs normally mediate immune responses and wound healing and, when upregulated, they can promote disease progression by remodeling tissue, activating signaling cascades, stimulating proliferation and migration, and by regulating adhesion. We identified Imaginal disc growth factors (Idgfs), orthologs of human CLPs CHI3L1, CHI3L2, and OVGP1, in a proteomics analysis designed to discover factors that regulate tube morphogenesis in a *Drosophila melanogaster* model of tube formation. We implemented a novel approach that uses magnetic beads to isolate a small population of specialized ovarian cells, cells that nonautonomously regulate morphogenesis of epithelial tubes that form and secrete eggshell structures called dorsal appendages (DAs). Differential mass spectrometry analysis of these cells detected elevated levels of four of the six Idgf family members (Idgf1, Idgf2, Idgf4, and Idgf6) in flies mutant for *bullwinkle* (*bwk*), which encodes a transcription factor and is a known regulator of DA-tube morphogenesis. We show that, during oogenesis, dysregulation of Idgfs (either gain or loss of function) disrupts the formation of the DA tubes. Previous studies demonstrate roles for *Drosophila* Idgfs in innate immunity, wound healing, and cell proliferation and motility in cell culture. Here, we identify a novel role for Idgfs in both normal and aberrant tubulogenesis processes.

KEYWORDS morphogenesis; proteomics; imaginal disc growth factors; chitinase-like proteins; dorsal appendage

FLAT epithelia give rise to a stunning variety of tubular organs through mechanisms that are conserved from invertebrates to humans (Hogan and Kolodziej 2002; Lubarsky and Krasnow 2003; Berg 2008; Andrew and Ewald 2010), yet knowledge of the genetic and molecular underpinnings is limited. A tractable model for tubulogenesis in *Drosophila* is the formation of dorsal appendages (DAs) (Berg 2008), eggshell structures that facilitate gas exchange for the embryo (Figure 1A, left image). During oogenesis, DAs are secreted by cellular tubes that form in the egg chamber, which consists of 16 germline cells (1 oocyte and 15 nurse cells) surrounded by a somatic follicular epithelium (Figure 1, B and C). The somatic cells include columnar cells that cover the oocyte and squamous "stretch" cells that cover the nurse cells. Through a highly conserved wrapping mechanism, DA tubes form from two dorsal patches of columnar cells (Figure 1B) (Dorman *et al.* 2004; Ward and Berg 2005; Osterfield *et al.* 2013). These tubes elongate anteriorly by convergence and extension and by crawling over the adjacent stretch cells (Tran and Berg 2003; Ward and Berg 2005; Boyle and Berg 2009). The entire tube-forming process occurs in the absence of cell division or cell death (Dorman *et al.* 2004; Berg 2008). The tube-forming cells secrete eggshell protein into the tube lumens to make the DAs; the follicle cells then slough off when the egg is laid. Thus, the DAs serve as a read-out for proper tube formation, similar to the way that a Jell-O's shape reveals its mold.

Through live imaging, analysis of cell type-specific markers in fixed tissue, and mathematical modeling, we have a basic understanding of the tissue-level changes that make and

doi: https://doi.org/10.1534/genetics.116.199323
Manuscript received December 29, 2016; accepted for publication April 5, 2017; published Early Online April 12, 2017.
Supplemental material is available online at www.genetics.org/lookup/suppl/doi:10.1534/genetics.116.199323/-/DC1.
[1]Corresponding author: Department of Genome Sciences, University of Washington, Foege Bldg. S-433, Box 355065, 3720 15th Ave. NE, Seattle, WA 98195-5065. E-mail: caberg@uw.edu

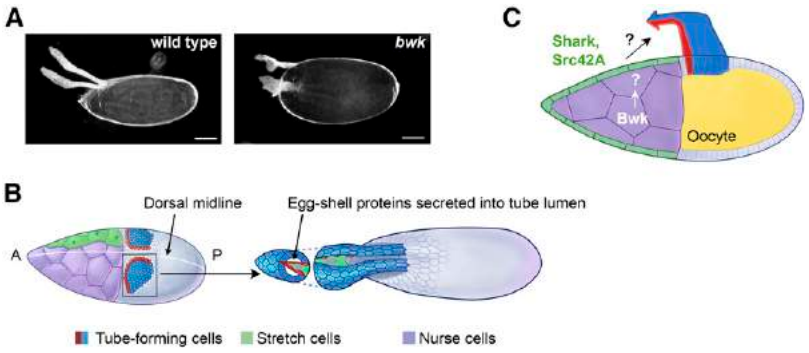

Figure 1 Distinct cell types interact to create dorsal appendage (DA)-forming tubes. (A) Laid eggs from wild-type (Canton S) and *bwk*-mutant females. (B) Squamous somatic follicle cells ("stretch" cells, green) surround 15 germline nurse cells (purple). Columnar somatic follicle cells (white, red, and blue cells) surround the oocyte. The red and blue cells form the tube, then elongate by migrating over the stretch cells. Tube cells secrete egg-shell proteins into the tube lumens to form each DA. A, anterior; P, posterior. (C) Regulation of DA morphogenesis by Bullwinkle (Bwk) from the nurse cells, and Shark and Src42A from the stretch cells. Shark and Src42A act downstream of Bwk. Signals between the cell types are unknown. Bar, 100 μm. (B and C) adapted from Dorman *et al.* (2004) with permission.

shape the DA tubes (Dorman *et al.* 2004; Osterfield *et al.* 2013; Peters and Berg 2016a). However, most of what we know about the regulation of this process comes from analyses of two mutants, *twin peaks* and *bullwinkle* (*bwk*), which disrupt expression of transcription factors required for tube morphogenesis (Rittenhouse and Berg 1995; French *et al.* 2003). Mosaic analyses demonstrate that Tramtrack69 (encoded by *tramtrack*), the BTB zinc finger protein affected in *twin peaks*, is needed in the first few rows of DA-forming cells to regulate tube elongation (Boyle and Berg 2009). In contrast, the SOX transcription factor Bullwinkle (Bwk) functions in the germline nurse cells to regulate DA formation (Rittenhouse and Berg 1995). Bwk controls tubulogenesis through the tyrosine kinases Shark and Src42A, which act in the overlying stretch cells (Figure 1C). Mutations in *bwk* or *Shark* lead to DA cell adhesion defects, aberrant cell migration, and open tubes, resulting in moose antler-like DAs (Rittenhouse and Berg 1995; Tran and Berg 2003; Dorman *et al.* 2004) (Figure 1A, right image). Other components of this signaling pathway, and the molecular signals and mechanical interactions between cell types that directly guide this anterior elongation and migration, are completely unknown. Here, we have begun to fill this void by using a proteomics analysis to identify additional molecules in the stretch cells that regulate tube morphogenesis.

To discover new components that function downstream of *bwk* to regulate tubulogenesis, we used mass spectrometry to identify proteins that are dysregulated in the stretch cells in *bwk* mutant egg chambers. We discovered that several members of a family of novel growth factors, Imaginal disc growth factors (Idgfs), were upregulated in *bwk* mutant egg chambers. A mass spectrometry approach in general provides advantages over other possible methods for gene discovery. First, potential genetic compensation and redundant function among members of a gene family can hamper detection, and indeed, Idgfs had gone undetected using large-scale, genome-wide, loss-of-function screens (Schüpbach and Wieschaus 1991; Spradling *et al.* 1999; Bellen *et al.* 2004). Second, like RNA-seq or microarray analyses, a mass spectrometry approach detects both upregulation and downregulation within the same analysis, providing information for genetic interaction due to either overexpression or loss of function. Third, mass spectrometry provides data for changes in protein levels or post-translational modifications, which can occur in the absence of changes in RNA levels. Thus, although the effort to purify a small population of cells for mass spectrometry analysis was considerable, the returns on this investment were exceptional.

In *Drosophila melanogaster*, six genes encode Idgfs: *Idgf1*, *Idgf2*, *Idgf3*, *Idgf4*, *Idgf5*, and *Idgf6* (Kirkpatrick *et al.* 1995; Kawamura *et al.* 1999; Bryant 2001; Varela *et al.* 2002). Idgfs are members of family 18 glycosyl hydrolases (GH18 family) and were originally identified and isolated from conditioned media from *Drosophila* S2 (Kirkpatrick *et al.* 1995) or imaginal disc cells (Kawamura *et al.* 1999). In imaginal disc cell culture (Clone 8 cells), Idgfs promote growth, proliferation, cell polarization, and motility (Kawamura *et al.* 1999). *Idgf* RNA is expressed in cells neighboring invaginating tissues during embryonic development (Kawamura *et al.* 1999), and some Idgf proteins are required for normal extracellular matrix (ECM) formation, larval and adult molting, or innate immune responses and wound healing (Kucerova *et al.* 2016; Pesch *et al.* 2016; Broz *et al.* 2017). The human orthologs, chitinase-3-like 1 (CHI3L1), chitinase-3-like 2 (CHI3L2), and oviductal glycoprotein 1 (OVGP1), are upregulated in several inflammatory disorders and cancers, and can induce proliferation and modulate cell adhesion and migration (Maines-Bandiera *et al.* 2010; Di Rosa *et al.* 2016). Although structurally related to chitinases, chitinase-like proteins (CLPs) such as the Idgfs and their human orthologs all share a conserved amino acid substitution in the catalytic domain that eliminates their ability to hydrolyze chitin, a major component of arthropod exoskeletons (Kawamura *et al.* 1999; Varela *et al.* 2002). Phylogenetic analyses suggest that the GH18 family originated from ancient genes (existing ~550 MYA) that underwent early duplications and subsequent mutations that allowed the CLPs to evolve new functions (Bussink *et al.* 2007; Funkhouser and Aronson 2007). The role of mammalian CLPs in normal developmental processes has not been explored. The present study establishes a role for Idgfs in a tube-formation mechanism that is conserved from invertebrates to humans.

Materials and Methods

Fly stocks

We used the following strains: *bwk^{151}/TM6 Hu* (Rittenhouse and Berg 1995), *bwk^{08482}/TM3 Sb* (Rittenhouse and Berg 1995), *c415-GAL4/TM3 Sb* (Manseau *et al.* 1997), *A90-GAL4* (Gustafson and Boulianne 1996), *A90-GAL4 bwk^{151}/TM3 Sb* (Tran and Berg 2003), *PG150-GAL4/FM7* (Bourbon *et al.* 2002), *w**; *shg*::*GFP* [endogenous E-Cadherin::GFP (Huang *et al.* 2009) via M. Osterfield], and *P{w$^+$, UAS-GFP.nls}14 P{w$^+$, tub-gal80[ts]}20* (gift from B. Edgar). We made the *c415-GAL4 bwk^{151}/TM3 Sb* strain by first locating the *c415-GAL4* transgene using plasmid rescue and sequencing (located at cytological location 77C7 in *CG4825* and upstream of *CG4858*) and then recombining it with the *bwk^{151}* chromosome. Expression of all of the Gal4 drivers used in these experiments begins in the stretch cells at stage 10, just prior to DA morphogenesis. Within egg chambers, *c415-GAL4* expression occurs exclusively in the stretch cells, except for (rarely) occasional single columnar follicle cell expression. *A90-GAL4* expression occurs in the stretch cells, the border cells, and in a few dorsal anterior columnar follicle cells. *PG150-GAL4* expression occurs exclusively in the stretch cells. The following strains are available from the Bloomington *Drosophila* Stock Center (BL) or the Vienna *Drosophila* Resource Center, (VDRC, V) and are described in FlyBase (http://flybase.org) (Gramates *et al.* 2017): Canton-S (BL64349), *w^{1118}* (BL3605), *UAS-GFP.nls14* (BL4775), *UAS-mCD8::GFP* (BL5137), *UAS-mCherry* RNAi (TRiP line, negative control; BL35785), *UAS-Idgf1* (overexpression; BL52657), *UAS-Idgf3* (overexpression; BL52658), *UAS-Idgf1* RNAi (GD line; V12414), *UAS-Idgf1* RNAi (TRiP line; BL57508), *UAS-Idgf2* RNAi (TRiP line; BL55935), *UAS-Idgf3* RNAi (GD line; V12423), *UAS-Idgf4* RNAi (GD line; V14624), *UAS-Idgf4* RNAi (TRiP line; BL55381), *UAS-Idgf4* RNAi (KK line; V104968), *UAS-Idgf5* RNAi (KK line; V100977), *UAS-Idgf6* RNAi (discontinued GD line; V12547), *UAS-Idgf6* RNAi (KK line; V100906), *UAS-Idgf6* RNAi (TRiP line; BL56905).

Cell separation and sample preparation

Flies of genotypes *w^{1118}*; *UAS-mCD8*::*GFP*; *c415-GAL4 +/TM3 Sb* or *w^{1118}*; *UAS-mCD8*::*GFP*; *c415-GAL bwk^{151}/bwk^{08482}* were reared at 25°. Females of both genotypes, along with male siblings, were collected on the day of eclosion and fed with wet yeast paste for ~48 hr at 25° prior to dissection. Ovaries were dissected in modified Ephrussi–Beadle Ringer's (EBR) solution and kept on ice in a 2.0-ml dolphin tube prior to cell separation. Ovaries were warmed (for ~10 min) to 25°, rinsed three times with room temperature PBS, and dissociated with 1 ml of 5.9 units/ml elastase (Sigma [Sigma Chemical], St. Louis, MO, E0258) per 200 ovaries for 1 min and 30 sec while gently triturating with a P1000 pipette tip. Next, 1 ml of ice-cold PBS was added and cells were centrifuged for 5 min at 250 × *g* in a swinging-bucket rotor of a refrigerated centrifuge, and then resuspended in 1 ml of ice-cold PBS. Cells were gently triturated for 5 min with a P1000 tip while being kept on ice. The single-cell solution was filtered through a Filcon 50-μm syringe type filter (Filcon, BD Pharmingen) into a clean 2-ml dolphin tube, centrifuged at 250 × *g* for 5 min, and resuspended in 135 μl of PBS per 200 ovaries. Next, 10 μl of magnetic beads [Miltenyi mouse CD8 (Ly2)-coated beads] were added per 90 μl of cell solution, gently mixed, and incubated for 15 min at 4–8° (not on ice, incubating on ice will slow down the binding of the beads to the cells). The cells were washed by adding 1–2 ml of PBS buffer, centrifuging at 250 × *g* for 5 min, and resuspending in 0.5 ml of PBS. A Miltenyi MACS separation column was placed in a magnet (Miltenyi magnet and stand) and equilibrated by applying 500 μl of PBS buffer. A 30-μm prefilter (Miltenyi) was rinsed two times with PBS, placed over the column, and the cell solution was applied through the prefilter into the column. The flow-through (unlabeled cells) was collected as a control. The labeled cells in the column were washed by adding 500 μl PBS buffer three times. The column was removed from the magnet and placed over a clean 2.0 ml dolphin tube. To collect the labeled (CD8+) cells, 750 μl of PBS was added to the column and the cells were flushed out with the supplied plunger. The magnetic bead protocol was adapted from a published protocol (Wang *et al.* 2006). A small sample of the cells was examined on the microscope removing 7.5 μl of cell solution and placing on a slide with 0.5 μl of 200 μg/ml propidium iodide. A coverslip with a dab of vacuum grease on each corner was placed over the cells and the total cells, dead cells, and GFP+ cells were counted. The purified fraction and the flow-through fraction (control) were centrifuged for 5 min at 250 × *g*. To concentrate the sample, nearly all of the PBS was removed, so that there was just a very thin layer of PBS covering the cell pellet. The cells were frozen immediately at −80°. After accumulating enough ovaries for three biological replicates for each genotype (~100 μg or 4000 ovaries per replicate), the cells were lysed by four cycles of thawing and freezing combined with sonicating in an ice-bath sonicator. The individual small samples were allotted into three replicates per genotype. The protein concentration was measured using a bicinchoninic acid (BCA) assay. Cell lysates were resuspended in 0.1% RapiGest (Waters Associates, Milford, MA) in 50 mM ammonium bicarbonate pH 7.8 and vortexed. Protein concentration was again measured with a BCA assay (Thermo Fisher Scientific). The sample was reduced with DTT (Sigma), alkylated with IAA (Sigma), and digested with trypsin (Promega, Madison, WI).

Mass spectrometry

Using one of three mass spectrometers, 1 μg of peptides was measured. Thermo LTQ-FT [data-dependent acquisition (DDA)], Thermo Q-Exactive (DDA), or Thermo Vantage [selected reaction monitoring (SRM)] coupled with a Waters Associates nanoACQUITY liquid chromatography system were used for these analyses. A 75-μm fused silica column (Polymicro Technologies) was packed with 15-cm C12 Jupiter (Phenomenex) 4-μm reverse-phase beads and a 100-μm fused silica Kasil (PQ Corporation) frit trap loaded with 4 cm

of C12 Jupiter. The gradient used for separation was a total of 90 min with buffer A containing 95% water, 5% acetonitrile, and 0.1% formic acid, and buffer B containing 95% acetonitrile, 5% water, and 0.1% formic acid. Three analytical replicates were run for each sample with each set of replicates randomized. Quality control samples were run every sixth sample and in the beginning of the runs to assess column chromatography stability. DDA data were searched with Sequest (Eng *et al.* 1994) against a *D. melanogaster* FASTA database from FlyBase (http://flybase.org, FB2012_04 Dmel Release 5.46) (Gramates *et al.* 2017) containing contaminants. False discovery rates were determined via a decoy database using Percolator (Kall *et al.* 2007) at a *q*-value threshold of 0.01 and peptides were assembled into protein identifications using an in-house implementation of ID Picker (Zhang *et al.* 2007) within MSDaPL (Sharma *et al.* 2012). SRM methods were assembled and data were analyzed with Skyline (MacLean *et al.* 2010).

We used a label-free method for assessing differential abundance. In our DDA analysis, differential protein abundance was inferred qualitatively by comparing normalized spectral counts (which correlates to abundance). We used the three biological replicates each of the *bwk vs.* wild-type samples to calculate a *P*-value using a *t*-test to rank the top 100 proteins (Supplemental Material, Table S1 in File S1). DDA quantitation has limitations, among which only the peptides of the highest abundance are selected for sequencing, leaving low-abundance peptides undetected, and the selection is stochastic so peptide detection can vary from run to run. We selected candidate proteins for further analysis from the top 100 proteins from the DDA analysis (including the *Idgf* proteins) and selected peptides to monitor in the SRM analysis (Figure 2, B and C, and Figure S2 in File S1).

Egg collections

Flies were reared and crosses set up at 25°, except for RNAi experiments using *PG150-GAL4* and *P{w+, UAS-GFP.nls}14 P{w+, tub-gal80[ts]}20*, for which flies were reared at 18°. For the egg collections, 20–50 female flies (1–4 days old) and 10–15 males (either siblings or w^{1118}) were placed on apple juice plates with a dab of wet yeast paste. For RNAi experiments, flies were shifted to 30° and aged for 24–48 hr prior to collecting eggs for analysis, except for RNAi experiments using *PG150-GAL4* and *P{w+, UAS-GFP.nls}14 P{w+, tub-gal80[ts]}20*, which were shifted from 18 to 30° and aged for 48–72 hr prior to collecting eggs for analysis. Plates were changed once daily for experiments involving bwk^{151}/bwk^{08482} transheterozygotes and twice daily for experiments involving bwk^{+}/bwk^{+} flies. Eggs were washed and mounted on slides with Hoyer's mounting medium (van der Meer 1977). Images were acquired using a Nikon Microphot FXA (Nikon, Garden City, NY) or an AmScope B690-PL. Images were processed using Photoshop CS (Adobe) and Helicon Focus (Helicon Soft).

Dual immunofluorescence and fluorescent in situ hybridization (IF/ FISH)

IF/FISH and probe generation were performed as described (Zimmerman *et al.* 2013), except that DEPC treatment was performed immediately following the first fixation, and the *in situ* probe for *Idgf5* used PCR to add T7 and SP6 RNA polymerase promoter sequences to linear DNA templates rather than cloning into a TOPO vector. To reveal cell shapes, we used mouse anti-α-Spectrin (3A9-concentrate, Developmental Studies Hybridoma Bank) at 1:100 (Dubreuil *et al.* 1987). DAPI was used at a concentration of 1 μg/ml. Probe concentrations for hybridization were all 1:500. We generated probes by amplifying sequences unique to each *Idgf* from Canton-S genomic DNA using the following primers:

Note: The GC-rich anchors (shown in lower case) were added to the PCR products as primer target sequences for adding T7 and SP6 promoter sequences in a second round of PCR. Ultimately, only the *Idgf5* probe template was generated by adding the T7 and SP6 and synthesizing the probe from the purified PCR product. We were unsuccessful in generating the rest of the *Idgf* templates using this method so we cloned them into TOPO vectors after one round of PCR (with the GC-rich anchors but without the T7 and SP6 sequences on the PCR product). T7: 5′-TAATACGACTCACTATAGGGAGAgggcgg-3′; SP6: 5′-ATTTAGGTGACACTATAGAAGAGgcgcgc-3′; *Idgf1* (most of last coding exon), FW (forward): 5′-gggcggCCAGGACGAACAGAATCGCT-3′, REV (reverse): 5′-gcgcgcGCCAGTGCAAAGTCCACG-3′, product size: 496 bp of genomic sequence (508 with GC-rich anchors); *Idgf2* (most of last coding exon), FW: 5′-gggcggAATGGCCTGGTGGACTTTGT-3′, REV: 5′-gcgcgcCCCTAGGTTCTTGACACGGG-3′, product size: 537 bp of genomic sequence; *Idgf3* (part of last coding exon and part of 3′-UTR), FW: 5′-gggcggATGGCAGGTCGTGGAAGATG-3′, REV: 5′-gcgcgcTTGTGACATTTGCGTGCTGG-3′, product size: 513 bp of genomic sequence; *Idgf4* (part of last coding exon and part of 3′-UTR), FW: 5′-gggcggAGGATTCGGGACTGACTGGA-3′, REV: 5′-gcgcgcCACAGGTTTGCGTTGAGTCA-3′, product size: 508 bp of genomic sequence; *Idgf5* (part of 5′ UTR part of first coding exon), FW: 5′-gggcggGCTAAGCGTTACTACCGTGC-3′, REV: 5′-gcgcgcCAAAACTCTGCGCATCGTAG-3′, product size: 141 bp of genomic sequence; *Idgf6* (part of last coding exon plus part of 3′-UTR), FW: 5′-gggcggAAAGGGCGACAATGGCATCT-3′, REV: 5′-gcgcgcTTCTTCACATGGTCAGCTATACA-3′, product size: 235 bp of genomic sequence.

All of the clones (*Idgf1*, *2*, *3*, *4*, and *6*) and the PCR product for *Idgf5* were verified by sequencing. Images were acquired using a Leica SP8X scanning confocal microscope. Images were processed using Photoshop (Adobe).

Live imaging

Idgf3-overexpression (*w**; *Ecadherin::GFP*; *c415-GAL4/UAS-Idgf3*) and control (*w**; *Ecadherin::GFP*; *c415-GAL4/TM3 Sb*) flies were reared at 25°. Upon eclosion, females along with males were shifted to 30° and fed wet yeast paste for 3 days before dissection of ovaries. Ovaries were dissected in Schneider's

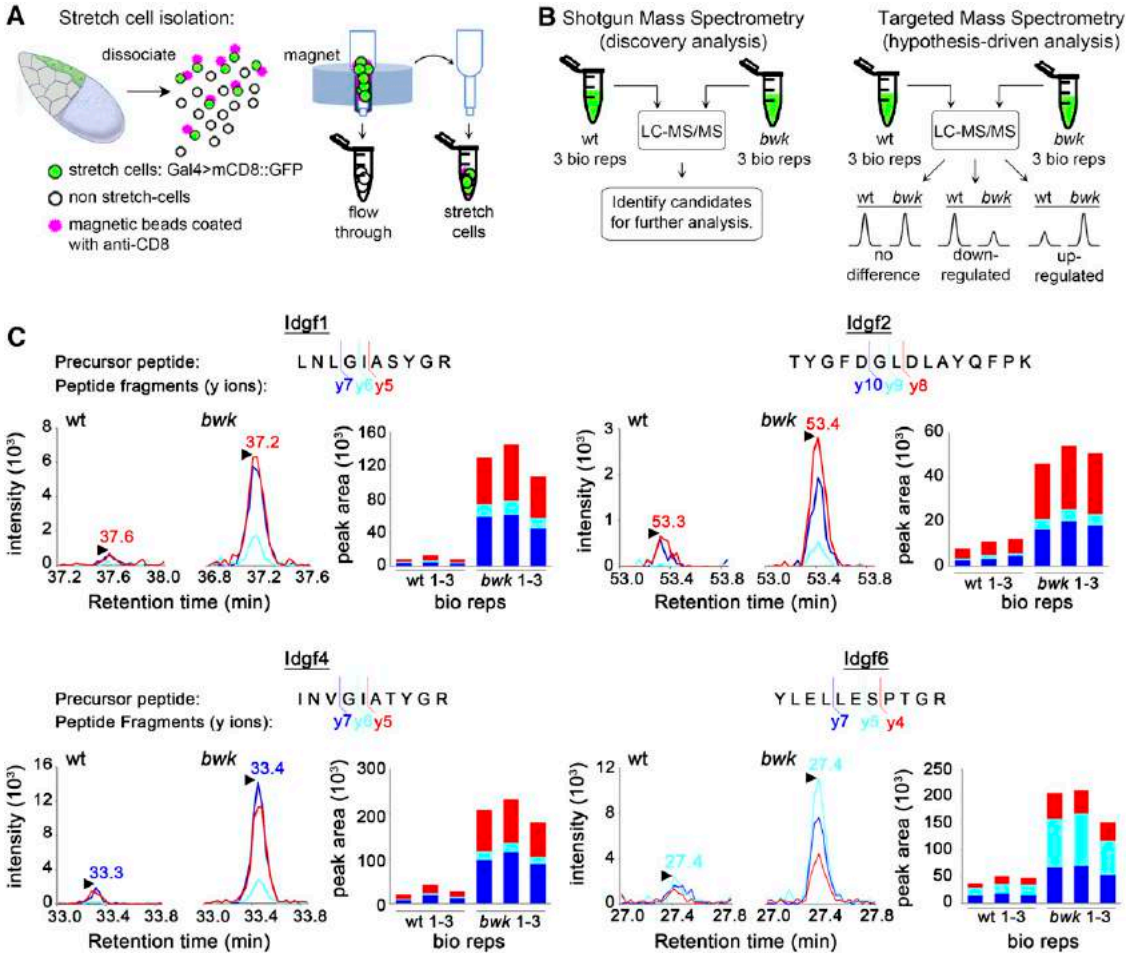

Figure 2 Cell separation and mass spectrometry. (A) Cell isolation. (B) Workflow for LC-MS/MS. Data-dependent acquisition ("shotgun") identified > 1000 proteins. Targeted mass spectrometry (selected reaction monitoring) estimated relative abundance of candidate proteins. (C) Chromatograms: relative abundance (intensities) and retention times of fragment ions. Bar graphs: total area under the fragment-ion peaks indicates higher relative abundance of Idgf peptides in stretch cells from *bwk* mutant females. y ions: y5 = 5-residue C-terminal fragment ion, etc. Peak areas were calculated by Skyline (MacLean *et al.* 2010) by integrating the area under the curves from the chromatograms. *bwk*, *bullwinkle*; Idgf, Imaginal disc growth factor; LC-MS/MS, liquid-chromatography tandem mass spectrometry; wt, wild-type.

medium (Thermo Fisher Scientific, Cat. No. 21720-024). Individual egg chambers were mounted on 35 mm Ibidi dishes (Cat. No. 81156) using a Kimwipe "blanket" to hold them in place, as described (Peters and Berg 2016b). Images were acquired on a Leica SP8X scanning confocal microscope and processed using Leica software (LAS Version X), FIJI (ImageJ Version 1.51j), and Photoshop (Version 12.1).

Data availability

The complete mass spectrometry data sets are downloadable from https://chorusproject.org/anonymous/download/experiment/383409849944218909 (DDA) and https://chorusproject.org/anonymous/download/experiment/-7610249330975803077 (SRM data). The Skyline SRM analysis files are available at https://panoramaweb.org/labkey/Skyline_Analysis_Idgfs.url. All other data required to confirm the main findings presented in the article are included with the article and in the Supplemental Material. File S1 contains supplementary tables and figures discussed in this manuscript. File S2, File S3, and File S4 are movies that depict live imaging of DA tubulogenesis as discussed in this manuscript. Fly strains are available from public stock centers or upon request.

Results

Idgf protein levels are elevated in stretch cells of bwk mutant egg chambers

To identify proteins that act in the stretch cells to regulate tube morphogenesis, we adapted a magnetic bead protocol (Wang *et al.* 2006) for use with mass spectrometry on stretch cells purified from wild-type and *bwk*-mutant ovaries (Figure 2A and Figure S1 in File S1); the *bwk* (bwk^{151}/bwk^{08482}) flies carry *P*-element insertions that reduce expression of *bwk*. We subjected unfractionated whole-cell extracts from the purified stretch cells to liquid chromatography coupled with tandem mass spectrometry (LC-MS/MS). The first phase of our analysis was discovery-based, using DDA or shotgun

proteomics (Figure 2B), which resulted in detection of over 1000 proteins (see Table S1 in File S1 for the top 100 proteins or https://chorusproject.org/anonymous/download/experiment/383409849944218909 for the complete data set). Next, in a hypothesis-driven phase, we manually selected candidate proteins from the discovery analysis for targeted mass spectrometry using SRM and assessed these peptides for differential abundance using Skyline (MacLean *et al.* 2010) (Figure 2B). We observed elevated levels of four Idgfs (Idgf1, Idgf2, Idgf4, and Idgf6) in the stretch cells of *bwk* mutant egg chambers (Figure 2C and Figure S2 in File S1). The Skyline SRM analysis files are available at https://panoramaweb.org/labkey/Skyline_Analysis_Idgfs.url. The raw SRM files are available at https://chorusproject.org/anonymous/download/experiment/-7610249330975803077.

In the DDA (discovery) analysis, Idgf4 was present among the top 100 differentially abundant proteins, while Idgf1, Idgf2, and Idgf6 were identified but not within the top 100. Idgf3 and Idgf5 were not identified in our initial DDA analysis. Since DDA involves stochastic sampling across a limited dynamic range, only the most abundant proteins are selected for identification; if proteins are not highly abundant, they may not be consistently detected in every mass spectrometry run. We did indeed detect Idgf3 and Idgf5; however, this was in a subsequent targeted (SRM) analysis. Noise in the data for these particular peptides precluded accurate quantitation such that we were unable to conclude whether these proteins were upregulated in egg chambers from *bwk* flies. Nevertheless, the identification of a novel family of growth factors, proteins that can induce the polarization of cells in culture (Kawamura *et al.* 1999), was an intriguing finding since it suggested a potential underlying molecular basis for the aberrant cell behaviors of the DA-tube-forming cells in *bwk* mutants.

Overexpression of Idgfs in a wild-type background disrupts DA-tube morphogenesis

To determine whether upregulation of Idgfs is sufficient to induce DA defects, we used the two publicly available Idgf-expression lines to overexpress either Idgf1 or Idgf3 in the stretch cells in a wild-type background; we then scored DAs based on the severity of the defects (Figure 3A and Table S2 in File S1). To assess the efficacy of overexpression, we used a weaker (*PG150-GAL4*) and a stronger (*c415-GAL4*) driver and two different controls (*UAS-mCD8::GFP* and *UAS-GFP.nls*); we also repeated each experiment twice and scored all samples blind to genotype. We found that Idgf3 overexpression dramatically increased the proportions of moderate and severe phenotypes (Figure 3A, graph). Idgf1 overexpression induced a smaller but statistically significant increase in DA defects in three out of the four experiments. Overexpression driven by the weaker Gal4 driver may have hovered closer to the threshold for inducing defects, whereas more robust overexpression driven by the stronger driver produced a more penetrant phenotype. Thus, stretch-cell overexpression of a single Idgf in an otherwise wild-type genetic background can mimic the loss-of-function phenotype of the transcription factor Bwk, a scenario in which four of the Idgfs are upregulated. This result suggests potential redundant function among Idgf family members.

In previous studies, we have extensively characterized the cellular dynamics of DA-tube formation in wild-type and *bwk*-mutant egg chambers (Tran and Berg 2003; Dorman *et al.* 2004; Osterfield *et al.* 2013). To examine the tissue phenotypes associated with Idgf3 overexpression during DA-tube morphogenesis, we imaged developing egg chambers from stage 11 through stage 14. In egg chambers overexpressing Idgf3 in the stretch cells, the roof-cell epithelium that forms the top of the tube was abnormally wide and short compared to wild-type egg chambers (see movies in File S2, File S3, and File S4, and compare Figure 3B with Figure 3C); this phenotype is strikingly similar to that of *bwk* mutants [see Figures 6 and 7 in Dorman *et al.* (2004)]. In wild-type chambers, the DA-tube cells wrapped to form a tight cone, then elongated rapidly to form a narrow stalk and flat paddle. In contrast, the roof cells in the Idgf3-overexpressing egg chambers migrated more slowly and exhibited impaired convergence and extension. When allowed to develop far longer than wild-type chambers, tube lumens were still substantially wider compared to control egg chambers (compare Figure 3B' with Figure 3C'), similar to the wide tube lumens of *bwk* mutants [see Figure 5 and Movie 3 in Dorman *et al.* (2004)]. These data support our observations on laid eggs that Idgf upregulation is sufficient to induce tube morphogenesis defects.

Idgf RNAi in a bwk background suppresses DA defects

Since Idgf overexpression can mimic the *bwk* phenotype, we reasoned that reducing Idgf expression downstream of *bwk* loss of function could suppress DA defects. To quantitate suppression, we measured DA length; shorter DAs are a consistent feature of eggs laid by *bwk* mothers and short DAs correlate with other aspects of the *bwk* phenotype, such as wider, wavier appendages (Tran and Berg 2003). We used stretch cell-specific RNAi in a *bwk* genetic background to knock down *Idgf4*, *Idgf5*, or *Idgf6* (RNAi constructs on the second chromosome available at the time) and observed an increase in average DA length (Figure 3D and Table S3 in File S1). DA lengths ranged from very short, as in *bwk* mutants (see graph in Figure 3D) to long, as on wild-type eggs (the median length of wild-type DAs is 280 μm). Although we did not quantify DA shape, we noticed that longer DAs tended to correlate with a more normal shape (Figure 3D). Note that *bwk* eggs always exhibit wide, short DAs, and this phenotype is 100% penetrant. We repeated these experiments using an alternative stretch cell-specific Gal4 driver and, when possible, alternative RNAi lines as they became available (Figure S3A in File S1). These results are consistent with the hypothesis that elevated levels of Idgfs contribute to the *bwk* phenotype.

Idgfs contribute to normal DA-tube morphogenesis

We questioned whether Idgf dysregulation can cause DA defects through a strictly gain-of-function mechanism or whether a minimal level of Idgf expression in the stretch cells

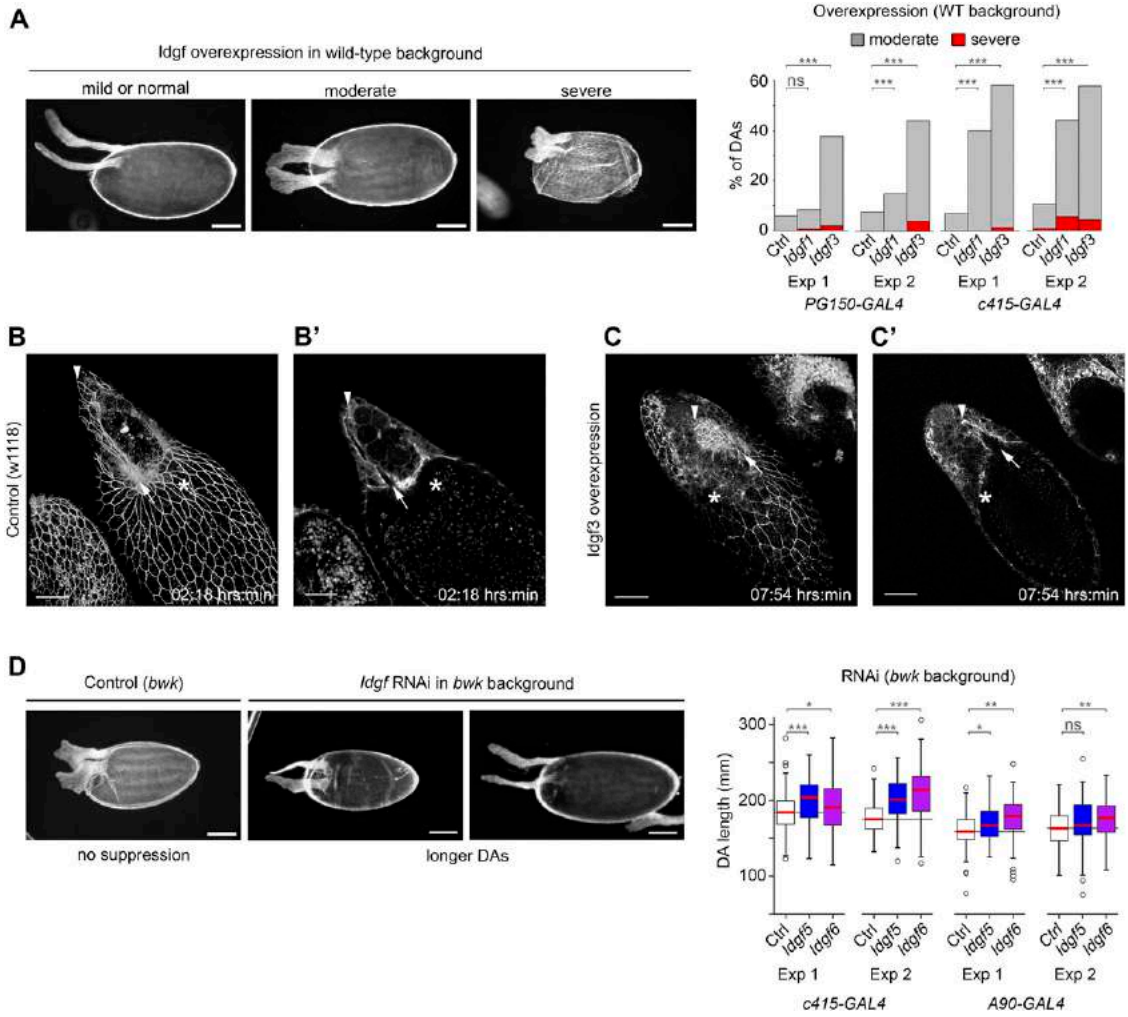

Figure 3 Elevated levels of Idgfs contribute to DA defects. (A) Stretch cell-specific Gal4-driven Idgf1 or Idgf3 overexpression induces DA defects. Representative phenotypic categories. Graph: proportions of moderate or severe DA phenotypes. Control: Gal4-driven GFP expression (GFP.nls for *c415-GAL4* Exp 2, mCD8::GFP for the rest). *N* for each genotype is given in Table S2 in File S1. ***$P < 0.001$, χ^2 test for trend in proportions (Rosner 2000). Significance was determined using the Benjamini–Hochberg procedure with FDR = 0.05. (B–C') Stills from movies in File S2 (B and B') and File S4 (C and C') at stage 13. Anterior is up and to the left. Asterisk indicates the dorsal midline. Ecadherin::GFP marks the adherens junctions of the follicle cells. (B) Genotype: *w*^{1118}; *Ecadherin::GFP*; +/+. The tube-forming cells have migrated over the stretch cells, forming a narrow stalk from the base (arrow) and a slightly widened paddle near the tip (arrowhead) (see movie in File S2). (B') Projection of interior optical planes shows the tube lumen underneath the roof cells. The base (arrow) and the tip (arrowhead) of the long, narrow tube are indicated. (C) Genotype: *w*^{1118}; *Ecadherin::GFP*; *c415-Gal4/UAS-Idgf3*. Migration of the tube-forming cells over the stretch cells is substantially impaired, resulting in abnormally short appendage primordia, even though the sample was allowed to develop hours longer than needed for WT tube development. Both the base (arrow) and tip (arrowhead) are abnormally wide (see movies in File S4 and File S3 for a second example). (C') Projection of interior optical planes shows the tube lumen underneath the roof cells. The base (arrow) and the tip (arrowhead) of the abnormally short, wide tube are indicated. (D) Suppression of *bwk* phenotype by RNAi. Stretch cell-specific RNAi knockdown of *Idgf5* or *Idgf6* in a *bwk* background (*UAS-Idgf* RNAi/+; *GAL4 bwk*^{151}/*bwk*^{08482}) suppresses the short-DA phenotype. Control: +/+ or CyO; *GAL4 bwk*^{151}/*bwk*^{08482} (*bwk* background with no RNAi). Boxplots show distribution of DA lengths. Whisker bars: range, hinges: 25th and 75th quantiles, red line = median, gray line = median of control, circles: outliers. *N* for each genotype is given in Table S3 in File S1 as well as data for additional RNAi lines. *$P < 0.05$, **$P < 0.01$, and ***$P < 0.001$, Welch's *t*-test. Significance was determined using the Benjamini–Hochberg procedure with a FDR of 0.05. Bar, 100 μm (A and D) and 50 μm (B–C'). *bwk*, *bullwinkle*; DA, dorsal appendage; Exp, experiment; FDR, false discovery rate; Idgf, Imaginal disc growth factor; ns, not significant; RNAi, RNA interference; WT, wild-type.

is necessary for normal DA morphogenesis. First, we asked which *Idgf* genes are expressed normally in the ovary. To detect expression in wild-type egg chambers, we used IF/FISH (Zimmerman *et al.* 2013), since validated antibodies against Idgfs were not available at the time of the writing of this paper. IF/FISH delineates stretch cells using a Spectrin antibody while simultaneously visualizing localization of *Idgf* transcripts. Transcripts for all six *Idgf* genes exhibit similar, punctate expression profiles in the stretch cells, but they have distinctly different profiles in the germline and columnar follicle cells, including a novel pattern in which two of the 15 nurse cells express *Idgf2* (Figure 4).

Stretch cell-specific RNAi with *PG150-GAL4* produced a modest but significant frequency of DA defects for each *Idgf*

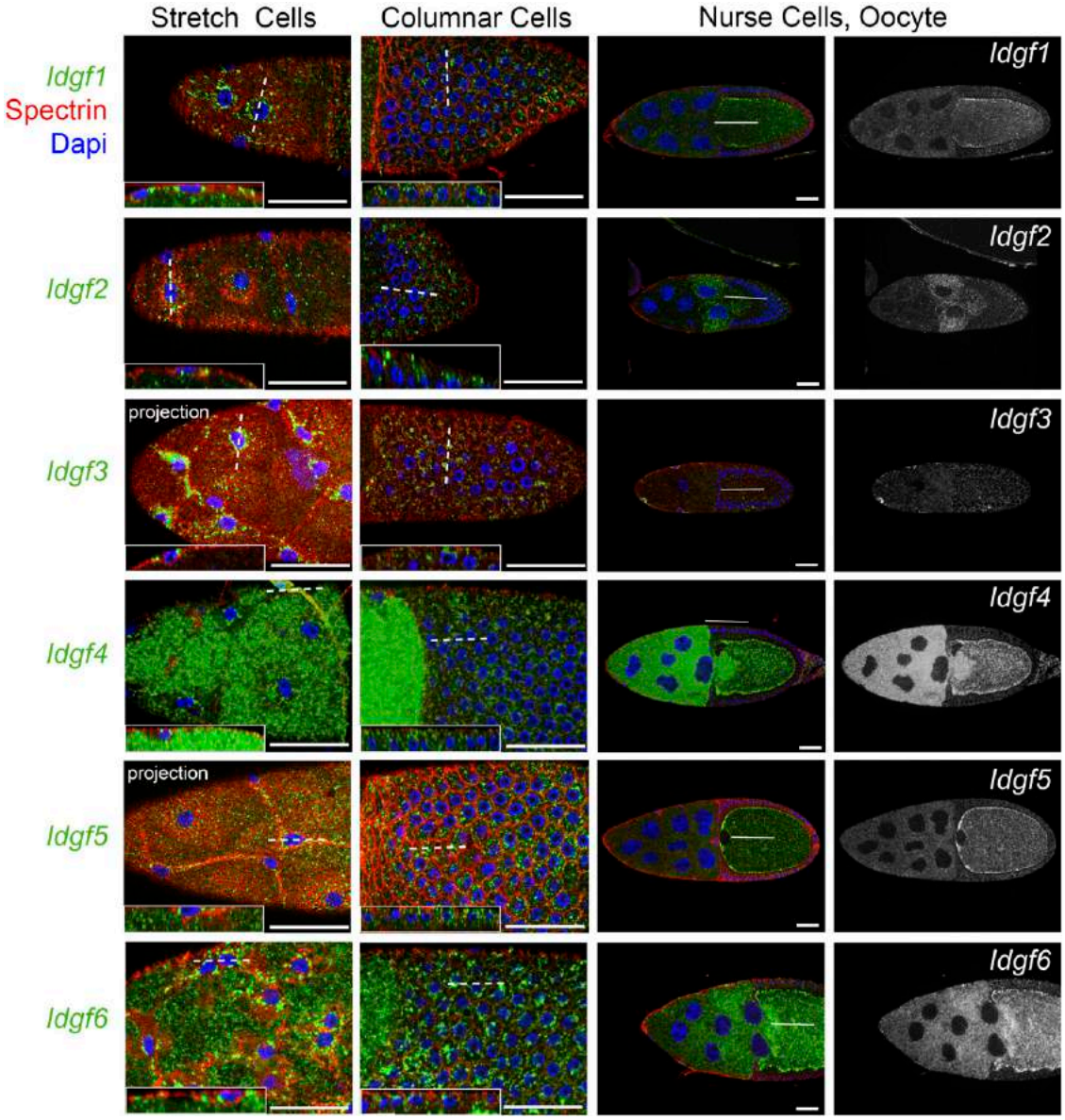

Figure 4 Wild-type cells express *Idgf* transcripts. Stretch cells in wild-type egg chambers, delineated by Spectrin protein (red), express RNA for all six *Idgf*s in a punctate pattern (green). DAPI (blue) marks the nuclei, which are highly polyploid in nurse cells (~2000 C) and less so in follicle cells (32–64 C). The dotted line indicates the location of the cross section shown in the inset. The solid white line indicates the dorsal midline. Punctate expression also occurs in the columnar cells. Nurse-cell expression differs between *Idgf*s. *Idgf2* has an unusual enrichment in the two dorsally-located nurse cells directly next to the oocyte. *Idgf4* and *Idgf6* have relatively high nurse-cell expression overall, and *Idgf*s *2*, *4*, and *6* transcripts appear to be transferred into the oocyte. *Idgf3* is distinctive with expression mostly if not entirely restricted to the stretch cells. *Idgf*s *1*, *4*, *5*, and *6* localize at or near the oocyte cortex. Bar, 50 μm. Idgf, Imaginal disc growth factor.

(Figure 5 and Table S4 in File S1). Since RNAi efficiency can vary with different Gal4 drivers and different RNAi constructs, we validated our results by performing the experiment twice using different stretch cell-specific Gal4 drivers, different controls, and, when possible, different RNAi constructs (Figure 5 and Figure S3B and Table S4 in File S1). As new RNAi constructs became available, we also tested those. For example, *Idgf2* RNAi was not available initially (Figure S3B in File S1) but was tested with the *PG150-GAL4* driver (Figure 5). While the results for *Idgf4*, *Idgf5*, and *Idgf6* RNAi were relatively similar in both experiments, the results for *Idgf1* and *Idgf3* RNAi were more variable. This variation could result from differences in the expression or activity of each RNAi construct or the perdurance of these proteins. Nevertheless, in all cases, there was a statistically significant increase in DA defects. Although some of the RNAi constructs are predicted to interfere with other transcripts, in each instance the "off-target" is a single other *Idgf* gene; in no case is the off-target a chitinase-active member of the GH18 family or any other gene (see Table S5 in File S1 for the

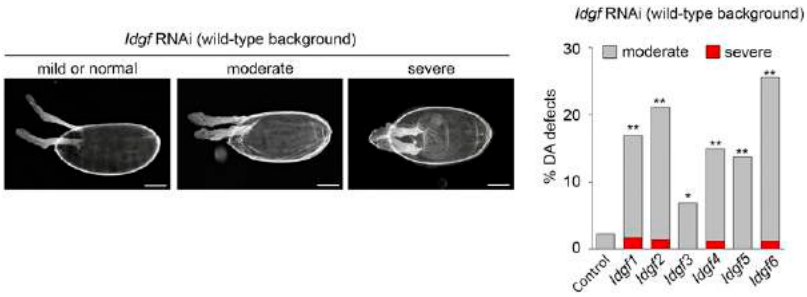

Figure 5 Reduction of *Idgf* expression produces DA defects. Stretch cell-specific knockdown of *Idgf*s (*PG150-GAL4>Idgf* RNAi) induces DA defects. Control: *PG150-GAL4>mCherry* RNAi. Left: Images show representative phenotypes. Right: Graph plots the proportions of DA phenotypes. $*P < 0.05$, $**P < 0.01$, χ^2 test for trend in proportions, $N = 218$ (control), 230 (*Idgf1*), 142 (*Idgf2*), 261 (*Idgf3*), 334 (*Idgf4*), 351 (*Idgf5*), and 247 (*Idgf6*). Significance was determined using Benjamini–Hochberg procedure with FDR of 0.05. Bar, 100 μm; DA, dorsal appendage; FDR, false discovery rate; Idgf, Imaginal disc growth factor; RNAi, RNA interference.

constructs with a predicted off-target transcript). These data are consistent with a hypothesis that Idgf proteins contribute to normal DA morphogenesis.

Discussion

We show that *Drosophila* Idgfs, orthologs of mammalian CLPs, have a role in the normal developmental process of tube formation and disrupt this process when overexpressed. These findings are quite remarkable because CLPs have no known role in tube formation in any system. Furthermore, although CLPs are upregulated in diverse disease contexts, the molecular mechanisms governing their effects, as well as the mutations that alter their levels, are unknown. Overall, our studies suggest that perturbations in DA morphogenesis occur when Idgf expression is not maintained at optimal levels in the stretch cells, with overexpression being particularly deleterious. Although many changes are likely occurring due to loss of *bwk* function in the nurse cells, we found that stretch-cell overexpression of a single Idgf, either Idgf1 or Idgf3, can mimic the *bwk* DA phenotype. Thus, these Idgfs are powerful modifiers of cell behavior. We predict that overexpression of the other Idgfs would have a similar effect on DA morphogenesis.

Interestingly, both overexpression and knockdown of individual Idgfs result in similar DA phenotypes. There are precedents for this phenomenon (Kelley *et al.* 2009; Wang *et al.* 2014). For example, reducing the amount of one component of a complex could compromise the function of the complex, resulting in a given phenotype. Overexpressing that same component, on the other hand, could disrupt the stoichiometry and squelch another component of the complex, compromising its function and resulting in the same phenotype. In the case of DA morphogenesis, polarization of tube-forming cells, properties of the stretch cells, tube formation, elongation by convergence and extension, and migration over the stretch cells may require precise coordination and timing. Disruption or faulty timing in any of these processes by nonoptimal levels of an Idgf, either by overexpression or knockdown, could result in wider, shorter, and/or misshapen tubes. Potential overlapping function between the six Idgf proteins could contribute to the incomplete penetrance in the RNAi experiments. The impact of reduction in the level of one Idgf in the stretch cells could be buffered by the presence of the other five Idgf proteins. Perdurance of Idgf protein could also be an issue; the Gal4 drivers do not express in the stretch cells until stage 10 of egg chamber development, after patterning has occurred but just hours before tube formation. Incomplete penetrance and variation in expressivity in any of our misexpression studies could be a result of Idgfs being close to a minimum or maximum threshold for proper tube morphogenesis, possibly making DA morphogenesis more sensitive to stochastic variation in the timing and coordination of events during tube formation and elongation. Another possibility is that Idgfs affect the expression of other genes in a network. Reducing expression of an Idgf could expose the process of DA-tube morphogenesis to stochastic variability in expression of the interacting gene, leading to incomplete penetrance. This type of phenomenon can occur in *Caenorhabditis elegans* during embryonic development (Raj *et al.* 2010).

How do Idgf proteins function in DA morphogenesis? One hypothesis is that Idgfs are involved in a signaling pathway that guides the DA-forming cells as they migrate over the stretch cells (Figure 6, A and B); their regulation could occur either through Shark and Src42A or through a parallel pathway, independent of Shark and Src42A. In this scenario, Idgf overexpression attracts DA cells in all directions, preventing proper tube closure and inducing aberrant migration (Dorman *et al.* 2004). This hypothesis is consistent with previous work showing that secreted Idgfs polarize cells and induce cellular extensions (Kawamura *et al.* 1999). Alternatively, Idgfs may affect cell adhesive properties or signaling by interacting with the ECM (Figure 6C). As lectins, Idgfs could be interacting with glycoproteins, which are abundant in the ECM. Idgfs may even signal in an autocrine fashion to modify the tensile or adhesive properties of the stretch cells (Figure 6D). Defects in stretch-cell surface proteins or ECM organization could impact the behavior of migrating DA cells, which contact the ECM as they migrate over the stretch cells.

Although the proteins that interact directly with the *Drosophila* Idgfs are unknown, a recent study found that *in vitro* treatment of Cl.8+ cells (cultured *Drosophila* wing imaginal disc cells) with recombinant Idgf2 transcriptionally upregulates a number of innate immunity genes, including *Attacin A*, *B*, and *D*, *Cecropin A1* and *A2*, *Drosocin*, *PGRP-LB*, and *Relish* (*relish*, *NF-κB*), the *Homeodomain interacting protein kinase*

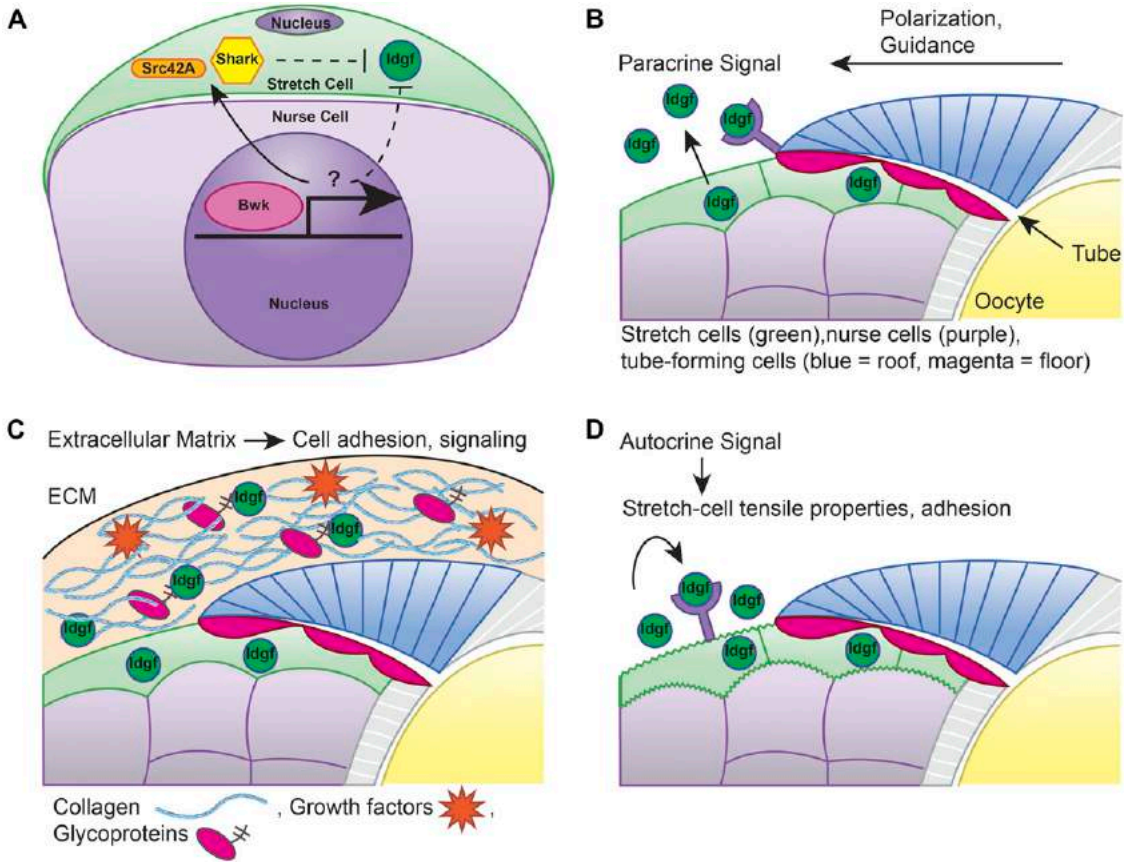

Figure 6 Hypotheses for Idgf function in DA morphogenesis. (A) Alternative signaling pathways downstream of Bwk transcriptional targets. A signal from the nurse cells to the stretch cells may regulate Idgf levels via Shark and Src42. Alternatively, Bwk may regulate levels of Idgfs through a pathway that is independent of Shark and Src42A. (B) Hypothesis 1: Idgfs are secreted from the stretch cells (green) and signal through a receptor in the tube-forming cells (blue and magenta), polarizing the tube-forming cells and guiding tube elongation. (C) Hypothesis 2: Idgfs are secreted into the extracellular matrix to regulate tube morphogenesis and cell migration through cell adhesion and signaling. (D) Hypothesis 3: Stretch cells secrete Idgfs and receive an autocrine signal that influences stretch cell tensile properties and adhesion to provide an optimal substrate for DA-cell migration. Bwk, Bullwinkle; DA, dorsal appendage; ECM, extracellular matrix; Idgf, Imaginal disc growth factor.

(*Hipk*) from the *Wnt* pathway, and *Zfh1* and *Mec2*, which are implicated in the function of nephrocytes (Broz *et al.* 2017). The same study showed that, in *Drosophila* larvae, Idgf2 protein localizes in pericardial cells and garland cells (nephrocytes). Mammalian studies may provide additional clues. Mammalian CHI3L1 activates both the mitogen-activated protein kinase (MAPK) and protein kinase B/AKT (PKB/AKT) pathways in fibroblastic cell culture (Recklies *et al.* 2002), and in murine macrophages and human cell lines it activates the Wnt/β-catenin pathway in addition to MAPK and PKB/AKT (He *et al.* 2013). Treatment of Cl.8+ cells with Idgf2 did not increase levels of phosphorylated Akt, but it is possible that one or more of the other Idgfs could activate Akt (Broz *et al.* 2017). CHI3L1 binds to the Interleukin-13 α2-receptor (IL13-Rα2), forming a multimeric complex with IL13-Ra2 and IL-13, and regulating apoptosis in mouse models of hyperoxia-induced lung injury (He *et al.* 2013). CHI3L1 physically interacts with the G protein-coupled receptor (GPCR) CRTH2 and promotes pulmonary fibrosis in mouse models of Hermansky–Pudlak syndrome (Zhou *et al.* 2015). By binding to RAGE (Receptor for Advanced Glycation Endproducts), a cell adhesion molecule (CAM) distantly related to Drosophila *robo1*, CHI3L1 promotes proliferation and survival of intestinal epithelial cells in inflammatory bowel disease and in colitis-associated cancer (Sessa *et al.* 2014; Low *et al.* 2015). MAPK, PKB/AKT, and Wnt/β-catenin pathway components, cytokines, GPCRs, and CAMs are candidate classes of proteins that may interact physically or genetically with Idgfs.

Our discovery-based proteomics analysis demonstrates the feasibility of assessing protein levels in a small subset of specialized cells, in this case, the squamous follicle cells (stretch cells), which are essential for tube morphogenesis in the *Drosophila* ovary. Despite the importance of stretch-cell function in tubulogenesis in the ovary, relatively little is known about protein expression and function in the stretch cells or how these cells facilitate tube morphogenesis. Our proteomics data provide a large trove of information previously unavailable for these unique cells and reveal the important roles of Idgfs in tube formation.

Acknowledgments

We thank the Bloomington *Drosophila* Stock Center and the Vienna *Drosophila* Resource Center for stocks, and FlyBase for genetic, polypeptide, and functional data. The α-Spectrin monoclonal antibody was obtained from the Developmental Studies Hybridoma Bank, created by the National Institute of Child Health and Human Development of the National Institutes of Health (NIH) and maintained by the University of Iowa, Department of Biology. We thank Nathaniel Peters at the University of Washington Keck Center for technical support and advice on imaging. We thank Anne Sustar, Liesl Strand, and other members of the Berg lab for helpful discussions. This work was supported by NIH grant R01-GM-079433 (C.A.B.), National Human Genome Research Initiative grant T32 H600035 "Interdisciplinary Training in Genomic Sciences" (S.G.Z.), and P41 GM-103533 (M.J.M.). The authors declare no competing interests.

Literature Cited

Andrew, D. J., and A. J. Ewald, 2010 Morphogenesis of epithelial tubes: insights into tube formation, elongation, and elaboration. Dev. Biol. 341: 34–55.

Bellen, H. J., R. W. Levis, G. Liao, Y. He, J. W. Carlson *et al.*, 2004 The BDGP gene disruption project: single transposon insertions associated with 40% of Drosophila genes. Genetics 167: 761–781.

Berg, C. A., 2008 Tube formation in *Drosophila* egg chambers. Tissue Eng. Part A 14: 1479–1488.

Bourbon, H. M., G. Gonzy-Treboul, F. Peronnet, M. F. Alin, C. Ardourel *et al.*, 2002 A P-insertion screen identifying novel X-linked essential genes in *Drosophila*. Mech. Dev. 110: 71–83.

Boyle, M. J., and C. A. Berg, 2009 Control in time and space: Tramtrack69 cooperates with Notch and Ecdysone to repress ectopic fate and shape changes during *Drosophila* egg chamber maturation. Development 136: 4187–4197.

Broz, V., L. Kucerova, L. Rouhova, J. Fleischmannova, H. Strnad *et al.*, 2017 *Drosophila* imaginal disc growth factor 2 is a trophic factor involved in energy balance, detoxification, and innate immunity. Sci. Rep. 7: 43273.

Bryant, P. J., 2001 Growth factors controlling imaginal disc growth in *Drosophila*. Novartis Found. Symp. 237: 182–194, discussion 194–202.

Bussink, A. P., D. Speijer, J. M. Aerts, and R. G. Boot, 2007 Evolution of mammalian chitinase(-like) members of family 18 glycosyl hydrolases. Genetics 177: 959–970.

Di Rosa, M., G. Distefano, K. Zorena, and L. Malaguarnera, 2016 Chitinases and immunity: ancestral molecules with new functions. Immunobiology 221: 399–411.

Dorman, J. B., K. E. James, S. E. Fraser, D. P. Kiehart, and C. A. Berg, 2004 *bullwinkle* is required for epithelial morphogenesis during *Drosophila* oogenesis. Dev. Biol. 267: 320–341.

Dubreuil, R., T. J. Byers, D. Branton, L. S. Goldstein, and D. P. Kiehart, 1987 *Drosophilia* spectrin. I. Characterization of the purified protein. J. Cell Biol. 105: 2095–2102.

Eng, J. K., A. L. McCormack, and I. Yates, 1994 An approach to correlate tandem mass spectral data of peptides with amino acid sequences in a protein database. J. Am. Soc. Mass Spectrom. 5: 976–989.

French, R. L., K. A. Cosand, and C. A. Berg, 2003 The *Drosophila* female sterile mutation *twin peaks* is a novel allele of *tramtrack* and reveals a requirement for Ttk69 in epithelial morphogenesis. Dev. Biol. 253: 18–35.

Funkhouser, J. D., and N. N. Aronson, Jr., 2007 Chitinase family GH18: evolutionary insights from the genomic history of a diverse protein family. BMC Evol. Biol. 7: 96.

Gramates, L. S., S. J. Marygold, G. D. Santos, J. M. Urbano, G. Antonazzo *et al.*, 2017 FlyBase at 25: looking to the future. Nucleic Acids Res. 45: D663–D671.

Gustafson, K., and G. L. Boulianne, 1996 Distinct expression patterns detected within individual tissues by the GAL4 enhancer trap technique. Genome 39: 174–182.

He, C. H., C. G. Lee, C. S. Dela Cruz, C. M. Lee, Y. Zhou *et al.*, 2013 Chitinase 3-like 1 regulates cellular and tissue responses via IL-13 receptor alpha2. Cell Rep. 4: 830–841.

Hogan, B. L., and P. A. Kolodziej, 2002 Organogenesis: molecular mechanisms of tubulogenesis. Nat. Rev. Genet. 3: 513–523.

Huang, J., W. Zhou, W. Dong, A. M. Watson, and Y. Hong, 2009 Directed, efficient, and versatile modifications of the *Drosophila* genome by genomic engineering. Proc. Natl. Acad. Sci. USA 106: 8284–8289.

Kall, L., J. D. Canterbury, J. Weston, W. S. Noble, and M. J. MacCoss, 2007 Semi-supervised learning for peptide identification from shotgun proteomics datasets. Nat. Methods 4: 923–925.

Kawamura, K., T. Shibata, O. Saget, D. Peel, and P. J. Bryant, 1999 A new family of growth factors produced by the fat body and active on *Drosophila* imaginal disc cells. Development 126: 211–219.

Kelley, D. R., D. J. Skinner, and C. S. Gasser, 2009 Roles of polarity determinants in ovule development. Plant J. 57: 1054–1064.

Kirkpatrick, R. B., R. E. Matico, D. E. McNulty, J. E. Strickler, and M. Rosenberg, 1995 An abundantly secreted glycoprotein from *Drosophila melanogaster* is related to mammalian secretory proteins produced in rheumatoid tissues and by activated macrophages. Gene 153: 147–154.

Kucerova, L., V. Broz, B. Arefin, H. O. Maaroufi, J. Hurychova *et al.*, 2016 The *Drosophila* chitinase-like protein IDGF3 is involved in protection against nematodes and in wound healing. J. Innate Immun. 8: 199–210.

Low, D., R. Subramaniam, L. Lin, T. Aomatsu, A. Mizoguchi *et al.*, 2015 Chitinase 3-like 1 induces survival and proliferation of intestinal epithelial cells during chronic inflammation and colitis-associated cancer by regulating S100A9. Oncotarget 6: 36535–36550.

Lubarsky, B., and M. A. Krasnow, 2003 Tube morphogenesis: making and shaping biological tubes. Cell 112: 19–28.

MacLean, B., D. M. Tomazela, N. Shulman, M. Chambers, G. L. Finney *et al.*, 2010 Skyline: an open source document editor for creating and analyzing targeted proteomics experiments. Bioinformatics 26: 966–968.

Maines-Bandiera, S., M. M. Woo, M. Borugian, L. L. Molday, T. Hii *et al.*, 2010 Oviductal glycoprotein (OVGP1, MUC9): a differentiation-based mucin present in serum of women with ovarian cancer. Int. J. Gynecol. Cancer 20: 16–22.

Manseau, L., A. Baradaran, D. Brower, A. Budhu, F. Elefant *et al.*, 1997 GAL4 enhancer traps expressed in the embryo, larval brain, imaginal discs, and ovary of *Drosophila*. Dev. Dyn. 209: 310–322.

Osterfield, M., X. Du, T. Schüpbach, E. Wieschaus, and S. Y. Shvartsman, 2013 Three-dimensional epithelial morphogenesis in the developing *Drosophila* egg. Dev. Cell 24: 400–410.

Pesch, Y. Y., D. Riedel, K. R. Patil, G. Loch, and M. Behr, 2016 Chitinases and Imaginal disc growth factors organize the extracellular matrix formation at barrier tissues in insects. Sci. Rep. 6: 18340.

Peters, N. C., and C. A. Berg, 2016a Dynamin-mediated endocytosis is required for tube closure, cell intercalation, and biased

apical expansion during epithelial tubulogenesis in the *Drosophila* ovary. Dev. Biol. 409: 39–54.

Peters, N. C., and C. A. Berg, 2016b *In vitro* culturing and live imaging of *Drosophila* egg chambers: a history and adaptable method, pp. 35–68 in *Oogenesis*, edited by I. P. Nezis. Springer, New York.

Raj, A., S. A. Rifkin, E. Andersen, and A. van Oudenaarden, 2010 Variability in gene expression underlies incomplete penetrance. Nature 463: 913–918.

Recklies, A. D., C. White, and H. Ling, 2002 The chitinase 3-like protein human cartilage glycoprotein 39 (HC-gp39) stimulates proliferation of human connective-tissue cells and activates both extracellular signal-regulated kinase- and protein kinase B-mediated signalling pathways. Biochem. J. 365: 119–126.

Rittenhouse, K. R., and C. A. Berg, 1995 Mutations in the *Drosophila* gene *bullwinkle* cause the formation of abnormal eggshell structures and bicaudal embryos. Development 121: 3023–3033.

Rosner, B. A., 2000 *Fundamentals of Biostatistics*. Duxbury Press, Pacific Grove, CA.

Schüpbach, T., and E. Wieschaus, 1991 Female sterile mutations on the second chromosome of *Drosophila melanogaster*. II. Mutations blocking oogenesis or altering egg morphology. Genetics 129: 1119–1136.

Sessa, L., E. Gatti, F. Zeni, A. Antonelli, A. Catucci *et al.*, 2014 The receptor for advanced glycation end-products (RAGE) is only present in mammals, and belongs to a family of cell adhesion molecules (CAMs). PLoS One 9: e86903.

Sharma, V., J. K. Eng, M. J. Maccoss, and M. Riffle, 2012 A mass spectrometry proteomics data management platform. Mol. Cell. Proteomics 11: 824–831.

Spradling, A. C., D. Stern, A. Beaton, E. J. Rhem, T. Laverty *et al.*, 1999 The Berkeley Drosophila Genome Project gene disruption project: single *P*-element insertions mutating 25% of vital Drosophila genes. Genetics 153: 135–177.

Tran, D. H., and C. A. Berg, 2003 *bullwinkle* and *shark* regulate dorsal-appendage morphogenesis in *Drosophila* oogenesis. Development 130: 6273–6282.

van der Meer, J. M., 1977 Optical clean and permanent whole mount preparation for phase-contrast microscopy of cuticular structures of insect larvae. Drosoph. Inf. Serv. 52: 160.

Varela, P. F., A. S. Llera, R. A. Mariuzza, and J. Tormo, 2002 Crystal structure of imaginal disc growth factor-2. A member of a new family of growth-promoting glycoproteins from *Drosophila melanogaster*. J. Biol. Chem. 277: 13229–13236.

Wang, P., Z. Zhou, A. Hu, C. Ponte de Albuquerque, Y. Zhou *et al.*, 2014 Both decreased and increased SRPK1 levels promote cancer by interfering with PHLPP-mediated dephosphorylation of Akt. Mol. Cell 54: 378–391.

Wang, X., J. Bo, T. Bridges, K. D. Dugan, T. C. Pan *et al.*, 2006 Analysis of cell migration using whole-genome expression profiling of migratory cells in the *Drosophila* ovary. Dev. Cell 10: 483–495.

Ward, E. J., and C. A. Berg, 2005 Juxtaposition between two cell types is necessary for dorsal appendage tube formation. Mech. Dev. 122: 241–255.

Zhang, B., M. C. Chambers, and D. L. Tabb, 2007 Proteomic parsimony through bipartite graph analysis improves accuracy and transparency. J. Proteome Res. 6: 3549–3557.

Zhou, Y., C. H. He, E. L. Herzog, X. Peng, C. M. Lee *et al.*, 2015 Chitinase 3-like-1 and its receptors in Hermansky–Pudlak syndrome-associated lung disease. J. Clin. Invest. 125: 3178–3192.

Zimmerman, S. G., N. C. Peters, A. E. Altaras, and C. A. Berg, 2013 Optimized RNA ISH, RNA FISH and protein-RNA double labeling (IF/FISH) in *Drosophila* ovaries. Nat. Protoc. 8: 2158–2179.

Communicating editor: M. F. Wolfner